ASTROBIOLOGY
Volume 13, Number 1, 2013
© Mary Ann Liebert, Inc.
DOI: 10.1089/ast.2012.0869

Radiation Resistance of Biological Reagents for *In Situ* Life Detection

Christopher E. Carr,[1,2] Holli Rowedder,[2] Cyrus Vafadari,[3] Clarissa S. Lui,[1] Ethan Cascio,[4] Maria T. Zuber,[1] and Gary Ruvkun[2,5]

Abstract

Life on Mars, if it exists, may share a common ancestry with life on Earth derived from meteoritic transfer of microbes between the planets. One means to test this hypothesis is to isolate, detect, and sequence nucleic acids *in situ* on Mars, then search for similarities to known common features of life on Earth. Such an instrument would require biological and chemical components, such as polymerase and fluorescent dye molecules. We show that reagents necessary for detection and sequencing of DNA survive several analogues of the radiation expected during a 2-year mission to Mars, including proton (H-1), heavy ion (Fe-56, O-18), and neutron bombardment. Some reagents have reduced performance or fail at higher doses. Overall, our findings suggest it is feasible to utilize space instruments with biological components, particularly for mission durations of up to several years in environments without large accumulations of charged particles, such as the surface of Mars, and have implications for the meteoritic transfer of microbes between planets. Key Words: Laboratory simulation experiments—Life-detection instruments—Nucleic acids—Mars—Panspermia. Astrobiology 13, 68–78.

1. Introduction

Nearly a billion tons of rock is estimated to have been transferred between Mars and Earth due to large meteorite impacts, mostly from Mars to Earth (Gladman and Burns, 1996; Gladman *et al.,* 1996). Of the several dozen meteorites of martian origin discovered here on Earth, around 20% experienced only mild heating during ejection and impact (Weiss *et al.,* 2000; Fritz *et al.,* 2005; Shuster and Weiss, 2005). Hypervelocity impact studies confirm that microbes can survive the required shock pressures (Horneck *et al.,* 2008). Given the possibility that viable microbes were transported between the planets, life on Mars, if it exists, may share a common ancestry with life on Earth.

We are building an instrument and developing protocols to test this hypothesis *in situ* on Mars by isolating, detecting, and sequencing nucleic acids (Ruvkun *et al.,* 2002; Isenbarger *et al.,* 2008a, 2008b). Our nominal approach relies on polymerase chain reaction (PCR) amplification as part of the sequencing process, because current single-molecule sequencing approaches are not yet suitable for space applications. The required reagents must function after months to years of space radiation exposure.

Many of these reagents, including enzymes, proteins, nucleotides, and dyes, have potential applications in other astrobiology investigations. For example, immunoassay (Parro *et al.,* 2011; Sims *et al.,* 2012) or oligonucleotide microarray approaches to life detection also utilize biological components (antibodies or nucleic acids) and fluorescent dyes. While these biochips avoid the complexity of PCR, they also lack its sensitivity. While immunoassays can target a variety of molecules, they are limited to a predefined set of targets and generally require a higher number of target molecules, whereas metagenomic sequencing can target any nucleic acid molecule. Oligonucleotide tiling microarrays also rely upon known or predicted sequences and suffer from high background noise. Tiles covering all possible sequences must be short and thus yield little new sequence information. Thus, immunoassay and metagenomic sequencing approaches are complementary; while the former offers a broader molecular diversity of predefined targets, the latter offers the potential for definitive and information-rich interrogation of any nucleic acid–based extant life.

To validate these reagents for use *in situ* on Mars and more generally in space, we exposed them to a variety of

[1]Department of Earth, Atmospheric and Planetary Sciences, Massachusetts Institute of Technology, Cambridge, Massachusetts.
[2]Department of Molecular Biology, Massachusetts General Hospital, Boston, Massachusetts.
[3]Department of Nuclear Engineering, Massachusetts Institute of Technology, Cambridge, Massachusetts.
[4]Francis H. Burr Proton Therapy Center, Massachusetts General Hospital, Boston, Massachusetts.
[5]Department of Genetics, Harvard Medical School, Boston, Massachusetts.

radiation sources selected to approximate the space radiation environment and compared their non-irradiated versus irradiated performance. We focused on radiation to the exclusion of other factors such as vibration or temperature because the former cannot be avoided and is essentially unique to the space environment. First, we briefly describe the main sources of space radiation and justify the target fluences or doses chosen for this study.

Space radiation is principally composed of galactic cosmic radiation (GCR) and solar radiation (Curtis and Letaw, 1989; Task Group on the Biological Effects of Space Radiation, 1996; Committee on Solar and Space Physics and Committee on Solar-Terrestrial Research, 2000; Committee on the Evaluation of Radiation Shielding for Space Exploration, 2008). By particle flux at peak during solar minimum, GCR consists of 90% protons (total flux $\sim 4\,cm^{-2}\,s^{-1}$), 9% helium ions (alpha particles), and 1% heavy ions (HZE) with a broad fluence peak near or below 1 GeV. Solar radiation is mainly composed of low-energy protons (<1 MeV, $10^{12}\ cm^{-2}\ s^{-1}$), solar storm protons (~1 MeV, $10^{5}\ cm^{-2}\ s^{-1}$), and solar flare protons (10 to 10^{3} MeV at 10^{5} to $10\,cm^{-2}\,s^{-1}$); the latter two are associated with a solar particle event (SPE). We neglect UV radiation because it can be blocked with minimal shielding. Energized electrons are principally a problem near planets with magnetic fields, such as in Earth's outer Van Allen belt, where high-energy solar wind electrons (0.1–10 MeV) can be trapped by interactions with Earth's magnetic field. The Van Allen belts also contain high-energy protons, up to $>10^{8}\ cm^{-2}\ s^{-1}$ at >0.1 MeV, or $<10^{3}\ cm^{-2}\ s^{-1}$ at >400 MeV, in the most intense regions. These high-energy protons have a flux versus energy profile similar to SPEs. Trips to Mars based on standard chemical propulsion will have transit times through the Van Allen Belts that limit their contribution to total dose.

The contribution of neutrons to the total radiation dose (10–60%) depends upon spacecraft shielding, as it is derived in large part from HZE secondary radiation (Bartlett *et al.,* 2006). Neutrons also contribute significantly to total dose on the surface of Mars; for example, the Mars Odyssey high-energy neutron detector mapped near-surface (<1 m depth) water on Mars by taking advantage of hydrogen's ability to moderate these secondary neutrons (Boynton *et al.,* 2002). Neutron fluxes at 1.5 m above the surface of Mars have been estimated as $80\,cm^{-2}\,s^{-1}$ (typical) or up to $145\,cm^{-2}\,s^{-1}$ during a SPE (Le Postollec *et al.,* 2009a, 2009b). The majority of martian neutrons' energies range from epithermal (10–1000 of keV) to fast (between 1 and 10^{4} MeV), with the bulk below 10 MeV and peaks at 0.6 and 6 MeV (Le Postollec *et al.,* 2009a).

Prior irradiation studies have tended to focus on the cellular through organism level or on nonbiological spacecraft components such as electronics and spacecraft materials. More recently, instruments have been proposed that involve chemical and biological components. For example, the Signs of Life Detector instrument (Parro *et al.,* 2005, 2011) and the Life Marker Chip (Sims *et al.,* 2012), payload concepts originally planned for the European Space Agency 2018 ExoMars mission, use antibodies to recognize protein domains and other biochemical structures. A related study (Le Postollec *et al.,* 2009a) demonstrated that antibodies and fluorescein dye were able to retain their function after 0.5 or 5 MeV neutron bombardment at a fluence equivalent to 1000 months on the surface of Mars. Also, exposure of the fluorescent dyes fluorescein and Alexa Fluor 633 to low-energy proton and alpha radiation, simulating unprotected exposure during a cruise to Mars, found that both dyes retained their fluorescent properties after irradiation (Thompson *et al.,* 2006). More recently, it was shown that antibodies and fluorophores survive Mars-relevant doses of gamma irradiation (de Diego-Castilla *et al.,* 2011), and DNA aptamers retain their binding affinity after 2 MeV proton exposure at fluences of 10^{9} to $10^{11}\ cm^{-2}$ (Baqué *et al.,* 2011).

2. Materials and Methods

2.1. Target fluence or dose

We selected target fluences or water-equivalent doses at levels conservatively above what would be expected for a 2-year mission duration (Table 1). We carried out a neutron exposure at the MIT Nuclear Radiation Laboratory (NRL), a proton exposure at the Massachusetts General Hospital (MGH) Burr Center for Proton Therapy, and a proton and heavy ion exposure at the Brookaven NASA Space Radiation Laboratory (NSRL) (Table 2).

For the MIT NRL neutron exposure, we selected a fluence above the worst-case scenario (145 neutrons $cm^{-2}\,s^{-1}$ during a SPE) for 2 years on the surface of Mars (Le Postollec *et al.,* 2009a, 2009b).

At MGH, we targeted the indicated fluences for two monoenergetic proton beams (25 MeV, 40 MeV), a high fluence polyenergetic SPE simulation (equivalent in dose to one day near Jupiter's moon Europa), and an extremely high fluence of 25 MeV protons (equivalent in dose to 2 or more years near Europa). For these proton exposures we controlled fluence. Proton fluence due to SPEs was based on the 370 known events over 2/1/1954 to 12/31/2007; weighting the event size by the predicted frequency [from Table 3 in Kim *et al.* (2009)] gives an approximate total fluence of 3×10^{9}

Table 1. Determination of Target Fluence or Dose

Particle	*Source*	*Flux* ($cm^{-2}\,s^{-1}$)	*Exposure time (years)*	*Fluence* (cm^{-2})	*Notes*	*Target fluence* (cm^{-2})
Proton	GCR	4	2	2.52×10^{8}	Mostly <1 MeV	4× nominal, 10^{9}
	SPE	$\leq10^{5}$	2	3×10^{9}	6.9 events/year	30× nominal, 10^{11}
HZE	GCR	0.04	2	2.52×10^{6}	Total HZE fluence	$>3\times10^{6}$
Neutron	Secondary	80	2	5.05×10^{9}	Mars surface, typical	2×typical, >worst case
	Production	145	2	9.15×10^{9}	Mars surface, SPE	1.00×10^{10}

Table 2. Summary of Exposures and Achieved Fluence or Dose

Source	*Facility*	*Particle*	*Energy (MeV/n)*	*Flux (cm^{-2} s^{-1})*	*Exposure time*	*Fluence (cm^{-2})*	*Dose (Gy)*
^{252}Cf	MIT	Neutron	ND	1.31×10^{5}	21:15:36	1.00×10^{10}	ND
Accelerator	MGH	H-1	25 [27]	ND	<1 min	1.01×10^{9}	3.6
Accelerator	MGH	H-1	40 [39]	ND	<1 min	1.01×10^{9}	2.6
Accelerator	MGH	H-1	SPE	ND	1.35 min	1.00×10^{11}	1.8×10^{2}
Accelerator	MGH	H-1	25 [27]	ND	3.75 h	3.4×10^{13}	1.2×10^{5}
Accelerator	NSRL	H-1	SPE	NA	4.25 min	5.4×10^{8}	1.0
Accelerator	NSRL	H-1	SPE	NA	11.88 min	2.7×10^{9}	5.1
Accelerator	NSRL	O-16	1000	2.5×10^{5}	2.97 min	4.4×10^{7}	1.0
Accelerator	NSRL	O-16	1000	4.8×10^{5}	7.56 min	2.2×10^{8}	5.0
Accelerator	NSRL	Fe-56	1000 [967]	4.6×10^{4}	1.48 min	4.1×10^{6}	1.0
Accelerator	NSRL	Fe-56	1000 [967]	4.9×10^{4}	6.95 min	2.1×10^{7}	5.0

Energy is target and [achieved] in MeV/nucleon; SPE indicates solar particle event energy distribution. ND, not determined; NA, not applicable. For non-NSRL exposures we controlled the fluence, while for NSRL exposures we controlled the water-equivalent dose, and the fluence and flux are calculated from linear energy transfer tables.

protons/cm^2 with energy ≥30 MeV for a 2-year mission. As a target, we chose a target exposure around 30-fold higher (10^{11}) to provide a margin of safety.

At NSRL, we targeted 1 and 5 Gy doses of 1 GeV oxygen and iron ions, and a proton SPE simulation (Supplementary Table S2; Supplementary Data are available online at www.liebertonline.com/ast) at similar doses. These heavy ion doses correspond to fluences above the total expected fluence of all HZE particles.

2.2. Neutron exposure

Samples were irradiated at the MIT Nuclear Radiation Laboratory by using a californium (^{252}Cf) source with reported emission 2.4×10^{8} s^{-1} and reported dose rates at 1 m in air of 2.31 mSv/h (neutron) and 0.168 mSv/h (gamma rays) at its original mass of 104.3 μg. Assuming quality factors of 10 and 1, respectively, these dose rates correspond to 0.23 and 0.17 mGy/h. The calculated emission rate was 1.64×10^{8} s^{-1} after adjustment for the exposure time ($t_{1/2}$ = 2.64 years, $t_{exposure}$ = 1.44 years after calibration). The desired neutron fluence was set at 10^{10} cm^{-2}, just above the worst-case estimate for 2 years on the surface of Mars, or around twice the typical fluence expected during this period.

We treated the source as a point mass located at the active end of the source and controlled the radial distance R of reagents from the source. Since californium also emits alpha particles, R should be greater than the distance an alpha particle will travel in air (~4 cm); in practice, alpha particles emitted within the source may be captured there as well. Second, R must be significantly smaller than the mean free path of a fast neutron in air (approximated as 78% nitrogen, 22% oxygen), which is ~20 m. Finally, to keep manufacturing costs low and limit sample exposure time we chose a small radius, R = 10 cm, giving an exposure time of 21.2 h.

We printed (Elite 3D, Dimension Printing) an ABS plastic tube rack with a spherical surface (Supplementary Fig. S1) to hold standard 1.5–2 mL tubes at this distance from the source. In practice, the ends of the tubes ranged from around 6.5 to 10 cm away from the source, so we can expect a 2.4× higher fluence at the base of a long tube relative to the estimate. The mean free path of a neutron also contributed to total variation in fluence: ^{252}Cf has a most probable neutron energy of 0.7 MeV and average neutron energy of 2.1 MeV (Hjalmar, 1955; Singleterry and Thibeault, 2000). In water, the neutron mean free paths at these energies are 2.3 and

Table 3. PCR Amplification Successful Except at Extreme Proton Doses

	MIT NRL	*MGH Burr Center*				*Brookhaven NSRL*					
Particle or ion	*Neutron*	*Proton (H-1)*				*Proton (H-1)*		*Oxygen (O-18)*		*Iron (Fe-56)*	
Energy (MeV/n)	*ND*[a]	*25*	*40*	*SPE*	*25*	*SPE*		*1000*		*1000*	
Dose (Gy)	*ND*	*3.6*	*2.6*	*1.8×10^{2}*	*1.2×10^{5}*	*1*	*5*	*1*	*5*	*1*	*5*
PCR Master Mix[b]	+	+	+	−	−	+	+	+	+	+	+
E. coli DNA	+	+	+	−	−	+	+	+	+	+	+
SYBR Green I	+	+	+	+	−	+	+	+	+	+	+
Taq polymerase	+	+	ND	+	−	ND	ND	ND	ND	ND	ND
PCR buffer	+	+	ND	+	−	ND	ND	ND	ND	ND	ND
dNTPs	+	+	ND	+	−	ND	ND	ND	ND	ND	ND
Primers	+	+	ND	−/+[c]	−[d]	ND	ND	ND	ND	ND	ND

Energy is target value. ND, not determined (because components worked together).
[a]Approximated by Maxwell distribution with beam energy 2.1 MeV, most probable energy 0.7 MeV.
[b]Master mix includes Taq polymerase, PCR buffer, dNTPs, primers (excludes template and SYBR Green I).
[c]Ribosomal primer 357F failed.
[d]Some nonspecific amplification occurred but no different than amplification observed with 357F primer alone, indicating off-target effect such as primer-dimer.

4.2 cm. Based on atomic cross sections, after 2 cm of liquid depth, the fluence may drop by up to a factor of 2.5× or 1.7×, respectively, but the fluence may decline by less than this estimate due to elastic scattering of neutrons in water. Thus, we can expect the portion of a sample closest to the source to be irradiated above our desired fluence and the portion near 10 cm to be irradiated below our target fluence in the worst case. Both radial position and neutron mean free path contribute to dose variability, but in terms of average dose these two effects oppose each other. Finally, samples experienced additional doses associated with gamma irradiation from the ^{252}Cf source and secondary production of gamma rays during elastic scattering of neutrons in water.

A 2.5 cm thick polystyrene sheet with a predrilled hole for the source was used to support the tube rack. After loading of samples, the rack was aligned to the source by using a predrawn circle on the sheet, and the rack and sheet were placed inside a cooler (Coleman Ultimate Extreme) on top of dry ice. Sample temperatures were measured before, during, and after the exposure (U12-015 HOBO temperature data logger, Onset Computer). Prior tests suggested that, due to poor air circulation, the air temperature could take longer than 30 min to transition from room temperature to below freezing, although once cold, temperatures would stay below freezing for several days. We dumped about 2 L room-temperature deionized water onto the dry ice before closing the lid, which caused CO_2 sublimation and indicated freezing temperatures within about 5–10 min (approximately the response time of the data logger in still air). During exposure, the temperature sensor was placed on the polystyrene sheet but away from the source. After the exposure, the samples were repackaged into a freezer box and stored on dry ice until they were returned to −20°C in the lab.

2.3. Proton irradiation at MGH

Samples were exposed to high-energy protons at the Francis H. Burr Proton Therapy Center at Massachusetts General Hospital by using a cyclotron that can accelerate protons up to 235 MeV. We generated near-monoenergetic beams (Supplementary Table S1) with target energies of 25 and 40 MeV and target fluence of 10^9 cm^{-2} (estimated dose 3.6 Gy). Briefly, the source beam (229 MeV) passes through a lexan degrader, a Lucite contoured scatterer (which helps flatten the beam profile), and an ion chamber, with air losses bringing the beam to near 39 MeV. An additional Lucite sheet (degrader) was used for the 25 MeV target condition to bring the beam to 27 MeV. Samples were placed immediately behind the degrader for the 25 [27] MeV beam and at the same position for the 40 [39] MeV beam. We used a diode cross to align the beam to achieve a flat region about 8 cm across (Supplementary Fig. S2). Samples in thin-walled (~0.25 mm) PCR tubes (polypropylene) were preloaded into the central 8×8 cm of thin-walled (~0.25 mm) polyethylene 96-well PCR plates. These plates were kept on ice except during exposure, when they were exposed to room temperature and proton-mediated heating. The four samples at the extreme corner positions may have experienced beam intensities 25–50% lower due to beam non-uniformity. For the SPE exposure, we used a rotating energy shifter as previously described (Cascio and Sarkar, 2008) to approximate the energy spectrum of the September 1989 SPE. When using the Burr Center accelerator, this energy shifter closely approximates the relative proton fluence of that event for energies from 35 to 205 MeV. We also performed an extreme exposure, using the 25 MeV target setup with a target fluence of 10^{14} cm^{-2}.

2.4. Proton and heavy ion irradiation at NSRL

Samples were irradiated at the NASA Space Radiation Laboratory at Brookhaven National Laboratory. Sample tubes were placed within a freezer box, and the outer row was loaded with water-filled tubes (Supplementary Fig. S3A). We used 1 GeV oxygen (O-16) and iron (Fe-56) ions generated by the Electron Beam Ion Source, and a proton SPE exposure was simulated by using the 200 MeV linear accelerator. Typical beam uniformity was <2% over a 13×13 cm area (Supplementary Fig. 3B–3D). The SPE exposure simulated the energy spectrum of the August 1972 SPE with the use of 11 monoenergetic beams from 50 to 150 MeV in 10 MeV increments; the full width at half maximum energy spread varied with the target energy level and ranged from 10–12 MeV at 50 MeV to 5 MeV at 150 MeV. Samples were kept in −20°C or on ice (cold packs) except during exposures and during activation checks. Additional beam characterization data is available online (http://www.bnl.gov/medical/nasa). Linear energy transfer values used to calculate water-equivalent dose (Supplementary Table S3) were determined with LET124 (http://tvdg10.phy.bnl.gov/let.html).

2.5. Reagents

In all irradiations, we included standard components of a PCR, including Taq polymerase and its associated PCR buffer (11647687001, Roche Diagnostics, Indianapolis, IN), deoxyribonucleotide triphosphate monomers (dNTPs, CB4420-2, Denville Scientific, South Plainfield, NJ), single-stranded DNA (ssDNA) primers targeting the ribosomal 16S gene (desalted custom oligos, Integrated DNA Technologies, Coralville, IA; for sequences see methods; volume varied depending upon synthesis yield, concentration 1 nmol/μL), and *Escherichia coli* genomic DNA (gDNA; 14380 10 MG, USB/Affymetrix, Inc., Santa Clara, CA). We also irradiated 100× SYBR Green I (diluted from S7585, Invitrogen, Carlsbad, CA), a dye that increases its fluorescence greatly upon binding double-stranded DNA (dsDNA), which is used to monitor amplification during quantitative (real-time) PCR (qPCR) (Zipper *et al.*, 2004), as well as a qPCR mastermix (iQ SYBR Green Supermix, 170-8880, Bio-Rad, Hercules, CA).

In the NSRL exposures, we also included lyophilized buffer, dNTPs, primers, gDNA, and a lyophilized master mix in an 8-PCR-tube strip format (High Yield PCR EcoDry Premix, ClonTech, Mountain View, CA). To study the effect of lyophilization during irradiation despite possible effects of lyophilization itself, we first lyophilized (Virtis FreezeMobile 25EL, SP Scientific, Gardiner, NY) matching reagent tubes and then rehydrated half of the tubes; because the EcoDry Premix was already lyophilized, we simply rehydrated some of the tubes before irradiation.

All reagents were expected to remain frozen during the brief exposures, with the exception of the longest-duration proton exposure at MGH. Reagents were used at commercially provided concentrations and volumes except as indicated above and in Supplementary Table S4.

2.6. Reagent performance assessment

We used qPCR as our primary method to assess reagent performance. After qPCR analysis, melt curves were used to visualize melting domains, and gel electrophoresis was used to visualize the expected band. For each exposure, we carried out a separate experiment, including both irradiated reagents and non-irradiated controls. We first ran qPCRs with all irradiated components and then tested individual components if a PCR failed or showed reductions in performance. As an added check, selected PCR products were sequence verified.

For historical reasons, PCR assays used all-bacterial ribosomal 16S primers 357F-19 (5′ CTC CTA CGG GAG GCA GCA G 3′) and 1492R-22-Y6 (5′ TAC GGY TAC CTT GTT ACG ACT T 3′) and *E. coli* purified DNA. This simulates targeted PCR for *in situ* life detection, although our nominal approach is metagenomic sequencing and, hence, is not limited by knowledge of specific sequences. Beginning experiments were performed on MBS satellite 0.2G Thermal Cycler (Thermo Electron Corp, Marietta, OH) with parameters consisting of 1 min at 95°C, 30 cycles of 15 s at 94°C, 30 s at 55°C, 1 min at 72°C and held for 7 min at 72°C. PCR products were run on 1% agarose gels in 1× TAE (40 m*M* Tris acetate, 1 m*M* EDTA) and visualized with ethidium bromide. Real-time PCR was performed with 0.5× SYBR Green I. Thermocycling (Bio-Rad CFX96 Real Time System, C1000 Thermocycler) parameters included 5 min at 95°C, 30 cycles of 10 s at 94°C, 30 s at 60°C, 2 min at 72°C; followed by 7 min at 72°C. A melt curve was performed at 65–95°C with 0.5°C × 5 s increments. Products were sequence verified through Sanger sequencing of amplicons with 16S reverse primer 907R-20-R15 (5′ CCG TCA ATT CCT TTR AGT TT 3′).

To assay for neutron-induced changes in SYBR Green I structure, we combined 25 or 40 μL 100× SYBR Green I with an equal volume of MeOH and injected into a Bruker Esquire 3000 Plus mass spectrometer in positive ion mode. We monitored a mass to charge (m/z) range of 50–1000 for 5 min.

3. Results

With the exception of the two highest-dose proton exposures, all conditions resulted in successful PCR amplification defined as the presence of the expected 1157 bp band during gel electrophoresis of each PCR product (Table 3). However, we observed some degradation in performance as described below.

3.1. Neutron irradiation

We detected no nuclear activation of the samples post-exposure. qPCR analysis revealed successful DNA amplification but some apparent degradation when all reagents were irradiated (Fig. 1A–1C, left). Samples with template (dark lines) generally amplified ~10 cycles before samples without template (light colors) (Fig. 1A–1B, 1E), indicating only minor contamination in the negative controls. Melt curve analysis revealed a single (expected) product in samples with template, and probable primer-dimer or low-level contamination in samples without template (Fig. 1C). When only a single irradiated reagent was included, qPCR curves were similar to the non-irradiated case except for SYBR Green I (Fig. 1A, center, orange curve), which was similar to the all-irradiated case. The converse was also true: when PCR reactions included all irradiated reagents except the one indicated reagent (Fig. 1A, right), only lack of irradiated SYBR Green I mimicked the non-irradiated case. Substitution of irradiated SYBR Green I caused a reduction in end-point fluorescence (Fig. 1D, orange to red curves), while substitution of all other irradiated reagents caused essentially no change in the qPCR curves (Fig. 1D, red to brown curves). This reduction in end-point fluorescence could be associated with concentration differences that could be driven in part by irradiation-induced destruction or photo bleaching. To search for evidence of SYBR Green I destruction, we analyzed irradiated and non-irradiated SYBR Green via mass spectroscopy and identified four main mass/charge peaks (Fig. 1F). The main peak at 509.3 matches the predicted exact mass of SYBR Green I ($C_{32}H_{37}N_4S+$, exact mass 509.27 amu); additional peaks at 255.1, 168.0, and 101.1 correspond closely to potential m/z peaks for charges $z = +2$ to $+4$. Thus, we found little evidence for neutron-induced damage to SYBR Green I at this fluence.

3.2. Proton irradiation at MGH

We found successful amplification after low-dose monoenergetic proton irradiation as demonstrated by real-time PCR, melt-curve analysis, and gel electrophoresis (Fig. 2). Tubes with DNA (dark) amplified earlier (Fig. 2A, 2C) than no-template controls (light) whether the master mix used was irradiated (red) or not (black). However, the 15.6 ± 4.9 (mean ± SD) cycle difference between DNA and no-template controls dropped to 7.1 ± 0.8 cycles after irradiation, due in part to critical cycle delay of 4.0 ± 0.4 cycles for the irradiated templates (Fig. 2E). Melt-curve analysis (Fig. 2B, 2D) revealed three melting domains, indicating primer-dimer, background contamination, and the expected ribosomal amplification products. In a separate experiment where only the DNA template was irradiated, we also found successful amplification (Fig. 2F). Monoenergetic proton exposure at 40 MeV gave similar results (not shown). In contrast, at 180 Gy with a SPE spectrum, proton irradiation resulted in an inability to amplify irradiated DNA template and an inconsistent ability to amplify non-irradiated DNA template when using irradiated primers (Table 3). The highest-proton-dose sample tubes were visibly yellowed, and due to activation, the sample was maintained at room temperature over 24 h. Tests in which these reagents were used uniformly failed to PCR. To confirm that this outcome was not simply due to storage at room temperature, we stored equivalent reagents at room temperature for 48 h before qPCR and found that all samples with template amplified successfully and all no-template controls failed to amplify (Supplementary Fig. S4).

3.3. Proton and heavy ion irradiation at NSRL

There was little impact of heavy ion irradiation on PCR (Fig. 3). Although there was variability in the qPCR end-point fluorescence (Fig. 3A, top row), after normalizing by end-point fluorescence, the qPCR curves were similar across all ions and doses (Fig. 3A, bottom row). The melt curves revealed a single melting domain in samples with template, and primer-dimer in no-template controls (Fig. 3B). In contrast, for the iQ SYBR Premix we found lower variation in end-point fluorescence (Fig. 3C), suggesting that end-point fluorescence differences

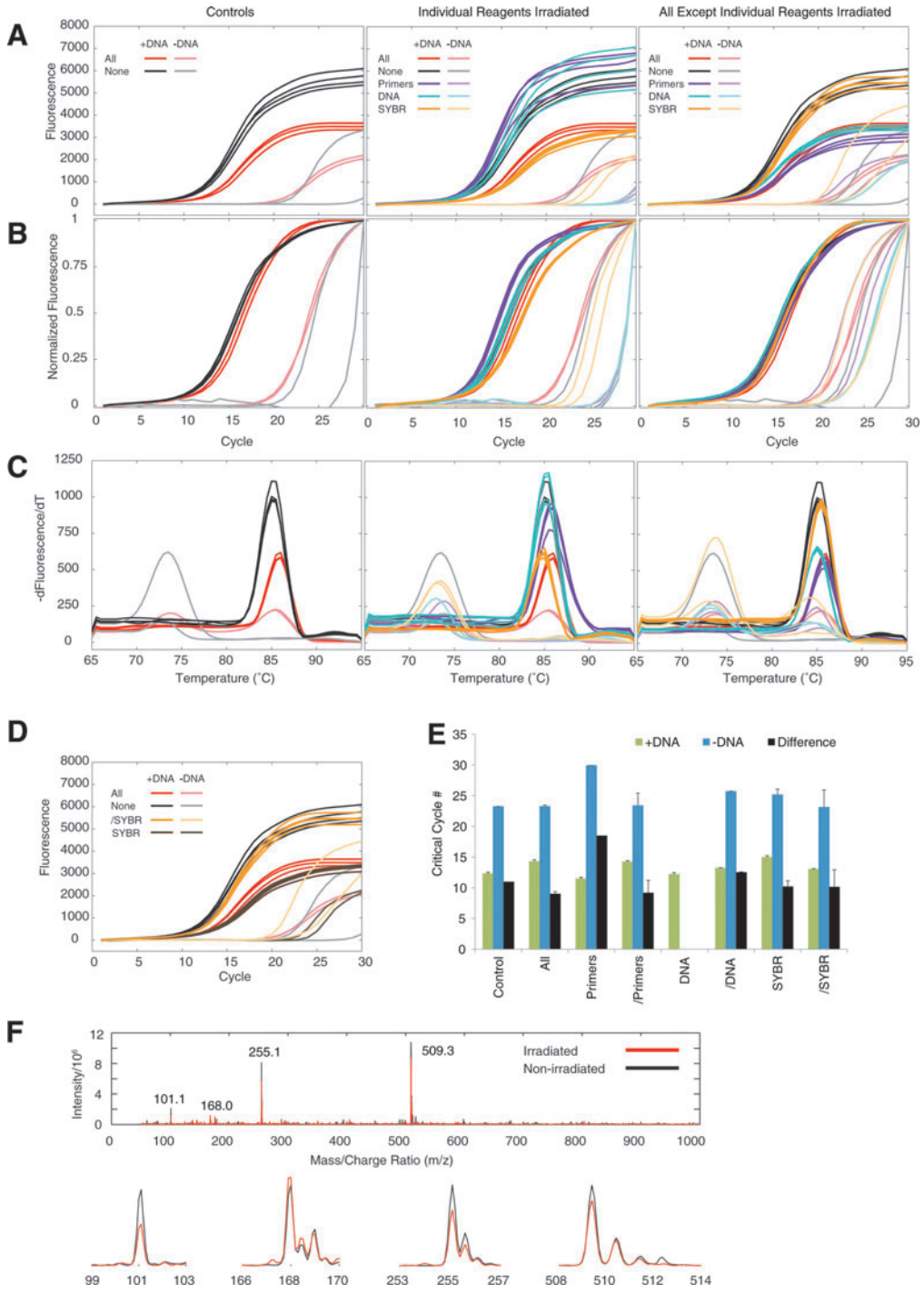

FIG. 1. Impacts of neutron irradiation. (**A**) qPCR amplification curves. (**B**) Curves in (A) normalized by end-point fluorescence. (**C**) Melt curve analysis of products from (A). (**D**) Curves from (A) comparing impact of irradiated SYBR Green I to irradiating all PCR components except SYBR Green I. (**E**) Critical cycle (Ct) values (/ indicates everything irradiated except indicated label). The DNA label's negative control did not amplify adequately for a Ct value to be determined. (**F**) Mass spectrometer analysis of SYBR Green I (top panel) reveals four main peaks (bottom panels) with little impact of irradiation. Vertical scale (intensity) in each bottom panel is arbitrary, but scaling is the same within each bottom panel for both irradiated and non-irradiated SYBR Green I. In all qPCR panels (A–D), no-template (−DNA) controls are light colors, while reactions with template (+DNA) are saturated colors.

result from variation in concentrations associated with pipetting rather than any impact of irradiation.

To identify the effects of irradiation on the exponential phase of PCR, we compared the critical cycle numbers of our non-premix qPCRs. For the non-premix PCRs, samples with template had critical cycle numbers 12–20 cycles lower than no-template controls (Fig. 3D); and a regression of ion, dose, and presence of template on critical cycle number revealed no effect of ion or dose ($p > 0.5$), with only the constant term and presence of template having significance ($p < 0.001$).

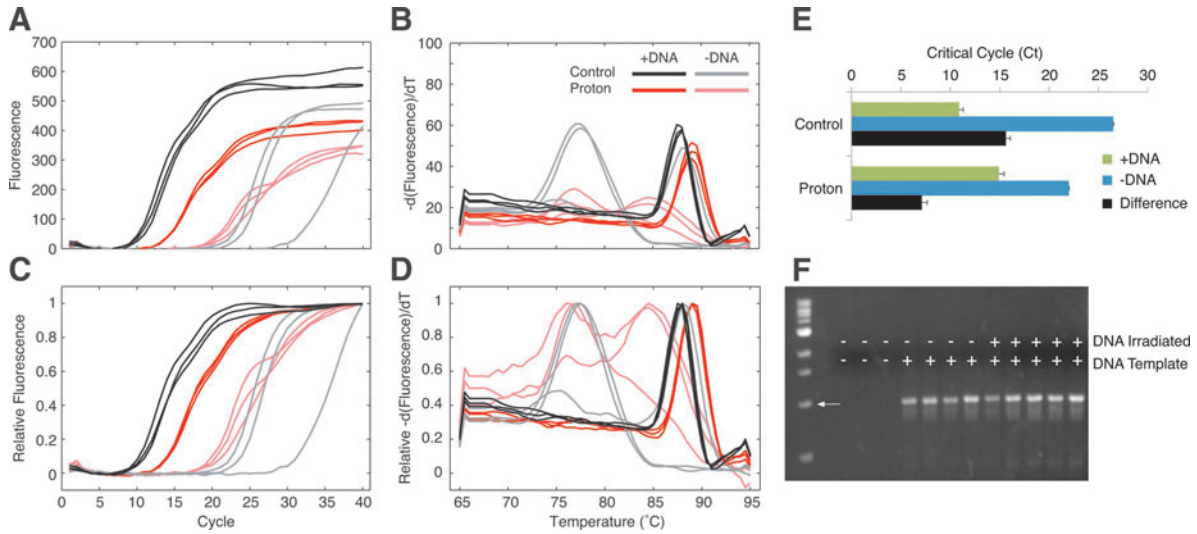

FIG. 2. Successful PCRs after monoenergetic proton irradiation. (**A**) qPCR of all-irradiated or non-irradiated reagents after 25 MeV proton exposure. (**B**) Melt curve analysis of (A). (**C**) Curves in (A) normalized by maximum fluorescence. (**D**) Melt curves normalized by maximum fluorescence. (**E**) Critical cycle values. (**F**) Gel electrophoresis of PCR products derived from gDNA irradiated by 40 MeV protons. Arrow indicates 1 kb band from NEB 1 kb ladder.

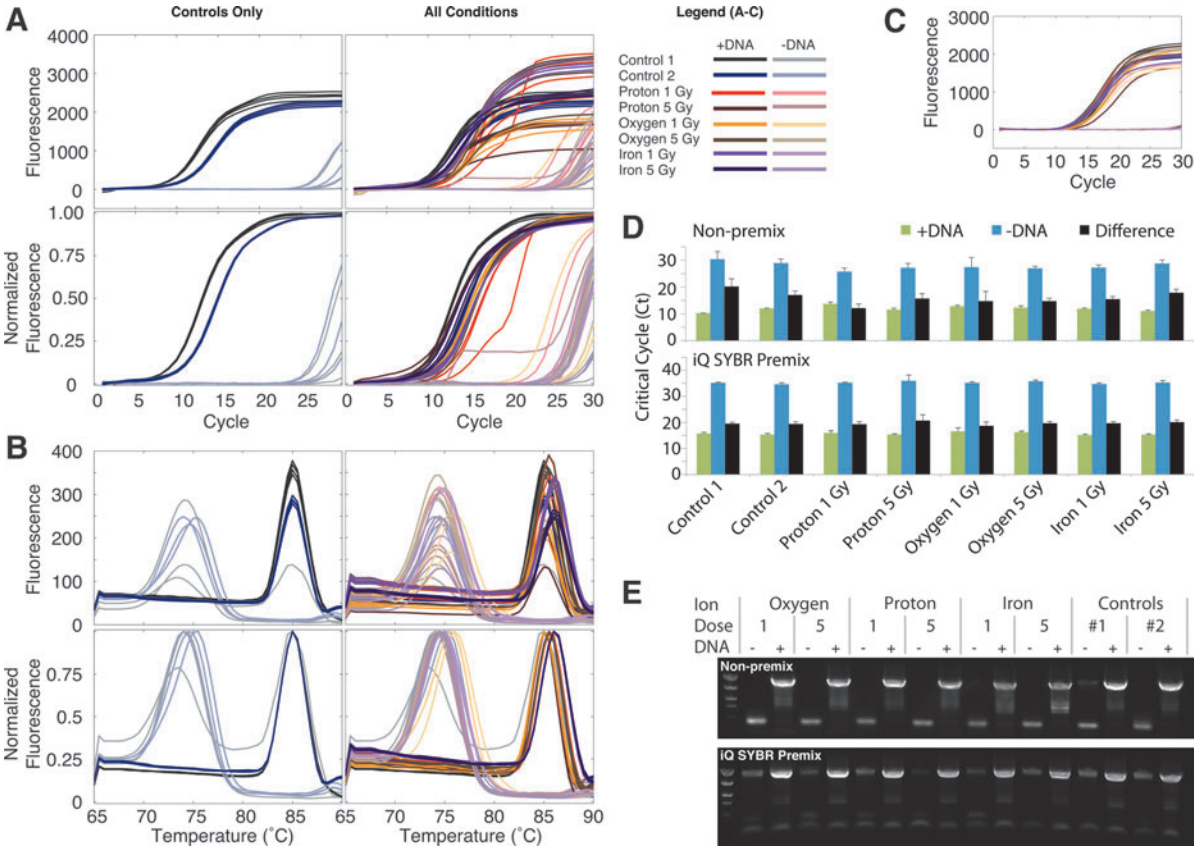

FIG. 3. PCR is robust to heavy ion irradiation. (**A**) qPCR amplification curves (top row) and same curves normalized by end-point fluorescence (bottom row) reveal successful amplification in samples with DNA template (dark) versus no-template controls (light). (**B**) Melt curve analysis of products from (A) reveals primer-dimer in no-template controls and expected ribosomal domain for samples with template. (**C**) qPCR end-point fluorescence variability is reduced when using iQ SYBR Premix. (**D**) Ion type and dose had no effect on critical cycle numbers. (**E**) Gel electrophoresis confirmed the expected product. Ladder: Lonza 50475 QuantLadder, with bands at 1500, 800, 400, 250, and 100.

Limiting the regression to samples with template reveals minor delays in critical cycle associated with irradiation (95% CI: 1.4–3.3, 1.4–3.2, and 0.3–2.1 cycles for proton, oxygen, and iron ions, respectively, with p values of <0.001, 0.012, and <0.001). However, in this regression, higher dose is associated with a lower critical cycle number (95% CI: -0.44 to -0.13, $p<0.001$), an improbable result that casts doubt on the significance of any ion or dose effect. A regression limited to no-template controls reveals a trend toward increased (2–4 cycles earlier) primer-dimer formation after irradiation (95% CI: -6.6 to -1.0, -5.9 to -0.3, and -5.1 to 0.5 cycles for proton, oxygen, and iron ions, respectively, with p values of <0.01, 0.10, and 0.03). For the iQ SYBR Premix, we found a similar lack of variation across ions and doses; the only significant coefficient other than the constant term or presence of template was found in a regression limited to samples with template, where oxygen ions were associated with a one-cycle delay (95% CI: 0.1–2.1 cycles, $p=0.03$). The small magnitude of this effect and the lack of any dose effect suggest no impact due to irradiation.

The expected products (in samples with template) and primer-dimer (in no-template controls) were then confirmed via gel electrophoresis (Fig. 3E). In comparison to the non-premix samples, the iQ SYBR Premix samples had a lower tendency to form primer-dimer and by 30 cycles had amplified some background contamination.

To evaluate the effect of lyophilization during proton and heavy-ion irradiation, we performed 30-cycle qPCR with the EcoDry Premix with added SYBR Green I and observed consistent amplification with some variability in end-point fluorescence (Fig. 4). This end-point variability is likely associated with pipetting of SYBR Green I, because this level of variability was not observed for the iQ SYBR Premix, which includes SYBR Green I. Regression analysis revealed no effect of ion or dose (all $p>0.2$). In contrast, the constant term, presence of template, and lyophilization were significant (all p values $<10^{-8}$). Hydration before irradiation was associated with a 0.9 cycle delay (95% CI: 0.7–1.1 cycles), indicating a possible, if tiny, benefit of lyophilization at the tested doses. However, this difference was also observed in the control conditions and may thus represent a small systematic bias instead of any benefit of lyophilization during irradiation. We also performed qPCR analysis with lyophilized individual reagents (buffer, primers, dNTPs, DNA, but not SYBR Green I) in a non-premix and identified no observable differences between lyophilized and hydrated reagents with a broad (15-cycle) difference in critical cycle numbers between samples with template and no-template controls (data not shown).

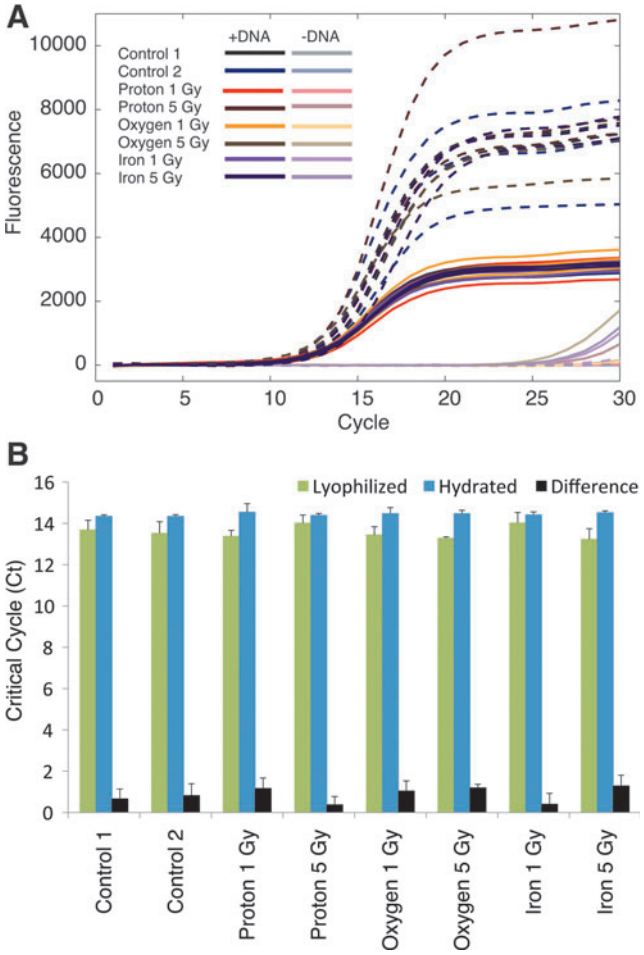

FIG. 4. Effects of lyophilization during proton and heavy ion irradiation. (**A**) qPCR amplification curves for hydrated (solid lines) and lyophilized (dotted lines) conditions. (**B**) Critical cycle numbers.

4. Discussion

4.1. Assessment of irradiation results

We demonstrate that PCR reagents are robust to neutron, proton, and selected heavy ion components of space radiation at a dose commensurate with a 2-year Mars mission.

We first validated californium as a source for future astrobiological studies of neutron bombardment. Of note, the most probable energy of 0.7 MeV closely matches the predicted 0.6 MeV peak on the surface of Mars (Le Postollec *et al.*, 2009a, 2009b). Californium also provides a gamma dose relevant to the radiation environment on Mars (de Diego-Castilla *et al.*, 2011). Our mass spectrometer analysis of irradiated SYBR Green I revealed that variability of end-point fluorescence was not necessarily an indicator of reduced dye performance. In later exposures, we continued to observe variability in end-point fluorescence despite careful control over the SYBR Green I concentration. Because we observed less variability in premix samples, this variability is likely to arise from relative concentration differences in the master mix associated with pipetting, leading to exhaustion of a limiting reagent at different concentrations of the final dsDNA product. Because we saw essentially no impact due to irradiation when using californium, we can conclude that neither the neutron nor the associated gamma dose impaired performance of our reagents.

Overall, we found little impact of the ions and doses tested except for the two highest-dose proton conditions. At the 180 Gy exposure with SPE energy levels, DNA (primers and gDNA) were inactivated by proton irradiation; this inactivation is unlikely to result from dsDNA breaks, as these can be expected to occur with a frequency of one per 10 Gy per 5×10^9 bases (Cox and Battista, 2005), or 0.02 per *E. coli* genome ($\sim5\times10^6$ bp). However, single-stranded breaks

occur with greater frequency, and the most likely source of inactivation may be nucleobase modification. Baqué *et al.* (2011) found that 2 MeV proton irradiation did not affect the function of DNA aptamers at fluences up to 10^{11} cm^{-2}. In contrast, we found inactivation of primers and gDNA at this fluence. This difference may result from the $>>2$ MeV energy protons used in our SPE simulation but may also result from increased sensitivity of the PCR assay relative to the aptamer assay. While PCR can be inhibited by a defect anywhere along the target region, local damage (such as base modifications or other lesions) does not necessarily disrupt the shape-recognition function of aptamers. Performing the aptamer assay with higher-energy protons or the PCR assay with 2 MeV protons should reveal the source of this difference.

Although we did not find any protective effect of lyophilization under the conditions tested, such stable storage will be beneficial to facilitate tolerance to temperature fluctuations, which will reduce mass, volume, and power requirements associated with reagent storage. Notably, de Diego-Castilla *et al.* (2011) found lyophilization or vacuum drying allowed fluorescence-conjugated antibodies to tolerate repeated sudden temperature shifts. In this study, we only tested lyophilization under low dose (1 and 5 Gy) proton and heavy ion exposure. It is likely that lyophilization would be protective at higher doses, where measurable decrements in PCR performance occur.

Our fluxes were much higher than would be expected during a Mars mission; however, we expect that any dose-rate effect is likely minimal due to the lack of damage sensing, damage repair, and the lack of heating except in the most extreme exposure. Because we demonstrated successful PCR when using non-irradiated reagents after 48 h of room-temperature storage (Supplementary Fig. 4), the complete inactivation of reagents at the highest proton dose is due to proton irradiation, not temperature. In this case, the complete failure of PCR at this dose places limits on the ability of life as we know it to survive during meteoritic exchange. In particular, under minimal shielding, typical SPE exposure, and no active repair, the high dose condition (and complete PCR failure) would be achieved within 23 thousand years, limiting the timescale of interplanetary transfer within ejecta particles too small to provide radiation shielding.

4.2. *Implications for* in situ *life detection*

In situ sequencing provides a sensitivity and specific approach to life detection of nucleic acid–based life. While challenging, extracting nucleic acids from Mars-like soils can likely be addressed (Lui *et al.,* 2011). While we focus here on the sequencing aspect, one promising approach with high contaminant rejection is synchronous coefficient of drag alteration (SCODA), in which rotating electric fields concentrate nucleic acids with extreme contaminant rejection (Broemeling *et al.,* 2008; Pel *et al.,* 2009).

Given this, how can we sequence *in situ?* Aside from single-molecule sequencing approaches (Eid *et al.,* 2009; Pushkarev *et al.,* 2009), which are impractical for our application due to their complexity, sequencing requires generating thousands to a million identical copies of the same DNA molecule. Of all commercially available sequencing technologies, semiconductor-based sequencing (Rothberg *et al.,* 2011) as commercialized by Life Technologies (Personal Genome Machine by Ion Torrent) enables concurrent sequencing in millions of wells; requires no imaging or optics; and is extremely small, fast, and robust. This approach requires PCR for clonal amplification on beads, followed by sequencing by synthesis with standard dNTPs and polymerase on a $\sim 3 \times 3$ cm semiconductor chip. As dNTPs are flowed over the millions of wells, detection occurs in each well by sensing the hydrogen ions released during nucleotide incorporation. Our results demonstrate that the principal reagents required for sequencing *in situ* can survive the space radiation expected during a 2-year Mars mission.

Reducing the extent of amplification required during sequencing is desirable for several reasons: First, amplification introduces bias in terms of the relative number of different sequences. Second, amplification can result in spurious results due to contamination or nonspecific amplification. Lesions caused by irradiation may increase the likelihood of nonspecific amplification. Ion Torrent has been scaling their technology toward smaller wells, which will require fewer clonal copies per bead, and this may reduce the required number of PCR cycles. A second possibility is an amplification-free sequencing technology such as nanopore strand sequencing (Oxford Nanopore), in which a dsDNA molecule is unzipped and passes in ssDNA form through a nanopore, changing the ionic current through the pore. Signal processing of current traces can be used to determine the base sequence, although the stated error rate is currently 4%. This technology is not yet commercially available but could permit strand sequencing without amplification, including for non-DNA polymers such as RNA. However, even the nanopore approach currently relies on biological components such as an alpha-hemolysin pore. Our study shows that at least one protein, Taq polymerase, is robust under the conditions studied, suggesting that other proteins like alpha-hemolysin may be adequately robust to be used in space-based life-detection applications. Beyond sequencing *in situ,* planned life-detection instruments contain biological components (Parro *et al.,* 2011). In addition, NASA has recently begun to explore space applications of synthetic biology; a critical prerequisite is that synthetic biology systems and the biological components of currently envisioned instruments must function despite space radiation.

Our results further support and expand the feasibility of using biological compounds in space, particularly for missions of short duration or in environments without large accumulations of charged particles. This includes our particular target of a 2-year Mars mission as well as other destinations under consideration for human exploration, such as lunar and asteroid missions. Recent discoveries of nucleic acids or their precursors within meteorites (Engel and Macko, 1997; Martins *et al.,* 2008; Schmitt-Kopplin *et al.,* 2010; Callahan *et al.,* 2011; Cooper *et al.,* 2011) and in interstellar space (Hollis *et al.,* 2000) could steer the development of life toward these biomolecules. Thus, it makes sense to search for RNA- or DNA-based life within potential habitable zones even outside the context of meteoritic exchange, such as the probable liquid water oceans beneath Europa (Carr *et al.,* 1998) and Enceladus (McKay *et al.,* 2008; *Postberg et al.,* 2011) and possibly Titan (Baland *et al.,* 2011). These environments may present more of a challenge: Our high-dose proton conditions correspond to 1 day and 2 years, respectively,

near Europa, suggesting that any mission there would require more robust reagents and/or significant shielding during any above-surface exposure. Our findings provide further evidence that meteoritic transfer of viable microbes to or from the jovian system is unlikely, given the small number of ejecta and the restriction that high dose rates place upon the residence time of such ejecta.

Acknowledgments

We thank Thomas Bork and William McCarthy for assistance with exposures at the MIT NRL, and Peter Guida, Adam Rusek, Michael Sivertz, and the rest of the NSRL-associated staff for assistance with heavy ion exposures. This work was funded by NASA's ASTID program (NNX08AX15G).

Author Disclosure Statement

No competing financial interests exist.

Abbreviations

dNTPs, deoxyribonucleotide triphosphate monomers; dsDNA, double-stranded DNA; GCR, galactic cosmic radiation; gDNA, genomic DNA; HZE, heavy ions; MGH, Massachusetts General Hospital; *m/z,* mass to charge; NRL, Nuclear Radiation Laboratory; NSRL, NASA Space Radiation Laboratory; PCR, polymerase chain reaction; qPCR, quantitative (real-time) PCR; SPE, solar particle event; ssDNA, single-stranded DNA.

References

Baland, R.M., Van Hoolst, T., Yseboodt, M., and Karatekin, Ö. (2011) Titan's obliquity as evidence of a subsurface ocean? *Astron Astrophys* 530:A141.

Baqué, M., Le Postollec, A., Ravelet, C., Peyrin, E., Coussot, G., Desvignes, I., Incerti, S., Moretto, P., Dobrijevic, M., and Vandenabeele-Trambouze, O. (2011) Investigation of low-energy proton effects on aptamer performance for astrobiological applications. *Astrobiology* 11:207–211.

Bartlett, D.T., Hager, L.G., and Tanner, R.J. (2006) Results of measurements on shuttle missions to the ISS of the neutron component of the radiation field. *Adv Space Res* 37:1668–1671.

Boynton, W.V., Feldman, W.C., Squyres, S.W., Prettyman, T.H., Bruckner, J., Evans, L.G., Reedy, R.C., Starr, R., Arnold, J.R., Drake, D.M., Englert, P.A.J., Metzger, A.E., Mitrofanov, I., Trombka, J.I., d'Uston, C., Wanke, H., Gasnault, O., Hamara, D.K., Janes, D.M., Marcialis, R.L., Maurice, S., Mikheeva, I., Taylor, G.J., Tokar, R., and Shinohara, C. (2002) Distribution of hydrogen in the near surface of Mars: evidence for subsurface ice deposits. *Science* 297:81–85.

Broemeling, D., Pel, J., Gunn, D., Mai, L., Thompson, J., Poon, H., and Marziali, A. (2008) An instrument for automated purification of nucleic acids from contaminated forensic samples. *JALA Charlottesville Va.* 13:40–48.

Callahan, M.P., Smith, K.E., Cleaves, H.J., Ruzicka, J., Stern, J.C., Glavin, D.P., House, C.H., and Dworkin, J.P. (2011) Carbonaceous meteorites contain a wide range of extraterrestrial nucleobases. *Proc Natl Acad Sci USA* 108:13995–13998.

Carr, M.H., Belton, M.J., Chapman, C.R., Davies, M.E., Geissler, P., Greenberg, R., McEwen, A.S., Tufts, B.R., Greeley, R., Sullivan, R., Head, J.W., Pappalardo, R.T., Klaasen, K.P., Johnson, T.V., Kaufman, J., Senske, D., Moore, J., Neukum, G., Schubert, G., Burns, J.A., Thomas, P., and Veverka, J. (1998) Evidence for a subsurface ocean on Europa. *Nature* 391:363–365.

Cascio, E. and Sarkar, S. (2008) A solar flare simulation wheel for the radiation test beamline at the Francis H. Burr Proton Therapy Center. *IEEE Transactions on Nuclear Science* 55:3428–3434.

Committee on Solar and Space Physics and Committee on Solar-Terrestrial Research. (2000) *Radiation and the International Space Station: Recommendations to Reduce Risk,* National Research Council, National Academies Press, Washington, DC.

Committee on the Evaluation of Radiation Shielding for Space Exploration. (2008) *Managing Space Radiation Risk in the New Era of Space Exploration,* National Research Council, National Academies Press, Washington, DC.

Cooper, G., Reed, C., Nguyen, D., Carter, M., and Wang, Y. (2011) Detection and formation scenario of citric acid, pyruvic acid, and other possible metabolism precursors in carbonaceous meteorites. *Proc Natl Acad Sci USA* 108:14015–14020.

Cox, M.M. and Battista, J.R. (2005) *Deinococcus radiodurans*—the consummate survivor. *Nat Rev Microbiol* 3:882–892.

Curtis, S.B. and Letaw, J.R. (1989) Galactic cosmic rays and cell-hit frequencies outside the magnetosphere. *Adv Space Res* 9:293–298.

de Diego-Castilla, G., Cruz-Gil, P., Mateo-Martí, E., Fernández-Calvo, P., Rivas, L.A., and Parro, V. (2011) Assessing antibody microarrays for space missions: effect of long-term storage, gamma radiation, and temperature shifts on printed and fluorescently labeled antibodies. *Astrobiology* 11:759–773.

Eid, J., Fehr, A., Gray, J., Luong, K., Lyle, J., Otto, G., Peluso, P., Rank, D., Baybayan, P., Bettman, B., Bibillo, A., Bjornson, K., Chaudhuri, B., Christians, F., Cicero, R., Clark, S., Dalal, R., deWinter, A., Dixon, J., Foquet, M., Gaertner, A., Hardenbol, P., Heiner, C., Hester, K., Holden, D., Kearns, G., Kong, X., Kuse, R., Lacroix, Y., Lin, S., Lundquist, P., Ma, C., Marks, P., Maxham, M., Murphy, D., Park, I., Pham, T., Phillips, M., Roy, J., Sebra, R., Shen, G., Sorenson, J., Tomaney, A., Travers, K., Trulson, M., Vieceli, J., Wegener, J., Wu, D., Yang, A., Zaccarin, D., Zhao, P., Zhong, F., Korlach, J., and Turner, S. (2009) Real-time DNA sequencing from single polymerase molecules. *Science* 323:133–138.

Engel, M.H. and Macko, S.A. (1997) Isotopic evidence for extraterrestrial non-racemic amino acids in the Murchison meteorite. *Nature* 389:265–268.

Fritz, J., Artemieva, N., and Greshake, A. (2005) Ejection of martian meteorites. *Meteorit Planet Sci* 40:1393–1411.

Gladman, B.J. and Burns, J.A. (1996) Mars meteorite transfer: simulation. *Science* 274:161–162.

Gladman, B.J., Burns, J.A., Duncan, M., Lee, P., and Levison, H.F. (1996) The exchange of impact ejecta between terrestrial planets. *Science* 271:1387–1392.

Hjalmar, E. (1955) Energy spectrum of neutrons from spontaneous fission of californium-252. *Physical Review* 100:1542–1543.

Hollis, J., Lovas, F., and Jewell, P. (2000) Interstellar glycolaldehyde: the first sugar. *Astrophys J* 540:L107–L110.

Horneck, G., Stöffler, D., Ott, S., Hornemann, U., Cockell, C.S., Moeller, R., Meyer, C., de Vera, J.P., Fritz, J., Schade, S., and Artemieva, N.A. (2008) Microbial rock inhabitants survive hypervelocity impacts on Mars-like host planets: first phase of lithopanspermia experimentally tested. *Astrobiology* 8:17–44.

Isenbarger, T.A., Carr, C., Johnson, S., Finney, M., Church, G., Gilbert, W., Zuber, M., and Ruvkun, G. (2008a) The most conserved genome segments for life detection on Earth and other planets. *Orig Life Evol Biosph* 38:517–533.

Isenbarger, T.A., Finney, M., Rios-Velazquez, C., Handelsman, J., and Ruvkun, G. (2008b) Miniprimer PCR, a new lens for viewing the microbial world. *Appl Environ Microbiol* 74:840–849.

Kim, M.-H.Y., Hayat, M.J., Feiveson, A.H., and Cucinotta, F.A. (2009) Prediction of frequency and exposure level of solar particle events. *Health Phys* 97:68–81.

Le Postollec, A., Coussot, G., Baqué, M., Incerti, S., Desvignes, I., Moretto, P., Dobrijevic, M., and Vandenabeele-Trambouze, O. (2009a) Investigation of neutron radiation effects on polyclonal antibodies (IgG) and fluorescein dye for astrobiological applications. *Astrobiology* 9:637–645.

Le Postollec, A., Incerti, S., Dobrijevic, M., Desorgher, L., Santin, G., Moretto, P., Vandenabeele-Trambouze, O., Coussot, G., Dartnell, L., and Nieminen, P. (2009b) Monte Carlo simulation of the radiation environment encountered by a biochip during a space mission to Mars. *Astrobiology* 9:311–323.

Lui, C., Carr, C.E., Rowedder, H., Ruvkun, G., and Zuber, M. (2011) SETG: an instrument for detection of life on Mars ancestrally related to life on Earth. In *Aerospace Conference, 2011 IEEE,* Institute of Electrical and Electronics Engineers (IEEE), Piscataway, NJ, doi:10.1109/AERO.2011.5747299.

Martins, Z., Botta, O., Fogel, M.L., Sephton, M.A., Glavin, D.P., Watson, J.S., Dworkin, J.P., Schwartz, A.W., and Ehrenfreund, P. (2008) Extraterrestrial nucleobases in the Murchison meteorite. *Earth Planet Sci Lett* 270:130–136.

McKay, C.P., Porco, C.C., Altheide, T., Davis, W.L., and Kral, T.A. (2008) The possible origin and persistence of life on Enceladus and detection of biomarkers in the plume. *Astrobiology* 8:909–919.

Parro, V., Rodríguez-Manfredi, J.A., Briones, C., Compostizo, C., Herrero, P.L., Vez, E., Sebastián, E., Moreno-Paz, M., García-Villadangos, M., Fernández-Calvo, P., González Toril, E., Pérez-Mercader, J., Fernández-Remolar, D., and Gómez-Elvira, J. (2005) Instrument development to search for biomarkers on Mars: terrestrial acidophile, iron-powered chemolithoautotrophic communities as model systems. *Planet Space Sci* 53: 729–737.

Parro, V., de Diego-Castilla, G., Rodríguez-Manfredi, J.A., Rivas, L.A., Blanco-López, Y., Sebastián, E., Romeral, J., Compostizo, C., Herrero, P.L., García-Marín, A., Moreno-Paz, M., García-Villadangos, M., Cruz-Gil, P., Peinado, V., Martín-Soler, J., Pérez-Mercader, J., and Gómez-Elvira, J. (2011) SOLID3: a multiplex antibody microarray-based optical sensor instrument for *in situ* life detection in planetary exploration. *Astrobiology* 11:15–28.

Pel, J., Broemeling, D., Mai, L., Poon, H.-L., Tropini, G., Warren, R., Holt, R., and Marziali, A. (2009) Nonlinear electrophoretic response yields a unique parameter for separation of biomolecules. *Proc Natl Acad Sci USA* 106:14796–14801.

Postberg, F., Schmidt, J., Hillier, J., Kempf, S., and Srama, R. (2011) A salt-water reservoir as the source of a compositionally stratified plume on Enceladus. *Nature* 474:620–622.

Pushkarev, D., Neff, N.F., and Quake, S.R. (2009) Single-molecule sequencing of an individual human genome. *Nat Biotechnol* 27:847–850.

Rothberg, J.M., Hinz, W., Rearick, T.M., Schultz, J., Mileski, W., Davey, M., Leamon, J.H., Johnson, K., Milgrew, M.J., Edwards, M., Hoon, J., Simons, J.F., Marran, D., Myers, J.W., Davidson, J.F., Branting, A., Nobile, J.R., Puc, B.P., Light, D., Clark, T.A., Huber, M., Branciforte, J.T., Stoner, I.B., Cawley, S.E., Lyons, M., Fu, Y., Homer, N., Sedova, M., Miao, X., Reed, B., Sabina, J., Feierstein, E., Schorn, M., Alanjary, M., Dimalanta, E., Dressman, D., Kasinskas, R., Sokolsky, T., Fidanza, J.A., Namsaraev, E., McKernan, K.J., Williams, A., Roth, G.T., and Bustillo, J. (2011) An integrated semiconductor device enabling non-optical genome sequencing. *Nature* 475:348–352.

Ruvkun, G., Finney, M., Church, G., Zuber, M., and Gilbert, W. (2002) A robotic-PCR detector for DNA-based life on other planets. In *Signs of Life: A Report Based on the April 2000 Workshop on Life Detection Techniques,* Committee on the Origins and Evolution of Life, National Research Council, National Academies Press, Washington, DC, pp 137–140.

Schmitt-Kopplin, P., Gabelica, Z., Gougeon, R., Fekete, A., Kanawati, B., Harir, M., Gebefuegi, I., Eckel, G., and Hertkorn, N. (2010) High molecular diversity of extraterrestrial organic matter in Murchison meteorite revealed 40 years after its fall. *Proc Natl Acad Sci USA* 107:2763–2768.

Shuster, D.L. and Weiss, B.P. (2005) Martian surface paleotemperatures from thermochronology of meteorites. *Science* 309:594–600.

Sims, M.R., Cullen, D.C., Rix, C.S., Buckley, A., Derveni, M., Evans, D., Miguel García-Con, L., Rhodes, A., Rato, C.C., Stefinovic, M., Sephton, M.A., Court, R.W., Bulloch, C., Kitchingman, I., Ali, Z., Pullan, D., Holt, J., Blake, O., Sykes, J., Samara-Ratna, P., Canali, M., Borst, G., Leeuwis, H., Prak, A., Norfini, A., Geraci, E., Tavanti, M., Brucato, J., and Holm, N. (2012) Development status of the life marker chip instrument for ExoMars. *Planet Space Sci* 72:129–137.

Singleterry, R.C. and Thibeault, S.A. (2000) Materials for low-energy neutron radiation shielding. NASA TP-2000-210281, National Aeronautics and Space Administration, Washington, DC.

Task Group on the Biological Effects of Space Radiation. (1996) *Radiation Hazards to Crews of Interplanetary Missions: Biological Issues and Research Strategies,* National Research Council, National Academies Press, Washington, DC.

Thompson, D., Wilson, P., Sims, M., Cullen, D., Holt, J., Parker, D., and Smith, M. (2006) Preliminary investigation of proton and helium ion radiation effects on fluorescent dyes for use in astrobiology applications. *Anal Chem* 78:2738–2743.

Weiss, B.P., Kirschvink, J.L., Baudenbacher, F.J., Vali, H., Peters, N.T., Macdonald, F.A., and Wikswo, J.P. (2000) A low temperature transfer of ALH84001 from Mars to Earth. *Science* 290:791–795.

Zipper, H., Brunner, H., Bernhagen, J., and Vitzthum, F. (2004) Investigations on DNA intercalation and surface binding by SYBR Green I, its structure determination and methodological implications. *Nucleic Acids Res* 32, doi: 10.1093/nar/gnh101.

Address correspondence to:
Gary Ruvkun
MGH Department of Molecular Biology
Simches Research Building
185 Cambridge Street
CPZN-7250
Boston, MA 02114

E-mail: ruvkun@molbio.mgh.harvard.edu

Submitted 20 April 2012
Accepted 24 September 2012